A Fault-Location Algorithm for Series-Compensated Double-Circuit Transmission Lines Using the Distributed Parameter Line Model

Ning Kang, *Member, IEEE*, Jiaxiong Chen, *Member, IEEE*, and Yuan Liao, *Senior Member, IEEE*

***Abstract*—A new fault-location algorithm for series-compensated double-circuit transmission lines utilizing two-terminal unsynchronized voltage and current measurements is presented in this paper. The mutual coupling between the parallel lines in the zero-sequence network is fully considered. The distributed parameter line model is adopted to fully take into account the shunt capacitance of the line. By formulating voltages and currents at the fault point in terms of the unknown fault location, boundary conditions under different fault types are used to derive the fault location. Two subroutines assuming the fault occurs on the left or right side of the series compensator are developed and the principle to identify the correct fault-location estimate is described. Matlab SimPowerSystems is employed to generate cases under diverse fault conditions for validating the proposed fault-ocation algorithm. Evaluation studies have shown that the proposed algorithm has achieved quite accurate results.**

***Index Terms*—Current phasors, double-circuit transmission line, fault location, series compensation, two terminal, voltage phasors.**

I. Introduction

THE SERIES compensation (SC) device is sometimes installed for long transmission lines to improve power transfer capability, enhance power system stability, damp power system oscillations, etc. The SC device can be a capacitor bank or thyristor-based power-flow controller, which is usually protected by a metal–oxide varistor (MOV) device. As is known, after a fault occurs, it is important to accurately locate the fault in order to quickly repair the faulted component and restore service [1]–[4]. In the past, fault-location algorithms for series-compensated lines have been developed based on synchronous or asynchronous data [5], [6].

Algorithms for single-circuit series-compensated transmission lines are described in [7]–[16]. Reference [7] puts forth a one-end fault-location algorithm using phase coordinates. In [8], based on the distributed time-domain model, two voltages are calculated from synchronized voltages and currents from two terminals and the fault distance is found to be the point where these two voltages are equal. Decoupled by modal transformation, a two-end unsynchronized fault-location technique based on the distributed parameter line model is presented in [9]. For [7]–[9], the calculation of voltage drop across the compensation device relies on the equivalent model of the SCs&MOVs. Reference [10] provides a time-domain two-end algorithm using the lumped parameter model with shunt and mutual capacitance ignored, where the instantaneous voltage drop across the compensation device is estimated. Reference [11] proposes a synchronous two-end algorithm based on the distributed parameter line model. Razzaghi *et al.* [12] extend the Electromagnetic Time Reversal theory to the fault location on the series-compensated multiconductor transmission lines. A fault-location method based on the distributed parameter line model for single-circuit transmission lines has been developed in [13]. Wavelet transform and neural-network techniques have been exploited to locate faults in [14]–[16].

Fault-location algorithms for double-circuit series-compensated transmission lines are reported in [17]–[21]. Maekawa *et al.* [17] describe two impedance-based fault-location methods using one-terminal and two-terminal measurements, respectively, which adopt the lumped parameter line model and ignore the shunt capacitances of lines. A one-end fault-location algorithm using phase coordinates has been proposed in [18], based on the lumped parameter model of the transmission lines. Reference [19] derives an analytical formula of the general fault loop, from which both fault location and fault resistance can be solved. The synchronization angle is computed in advance using prefault measurements or fault quantities. This paper adopts an approximate distributed parameter line modeling of the zero-sequence circuits and does not consider the exact zero-sequence mutual coupling between the two circuits. The authors of [20] propose an adaptive digital distance relaying scheme for intercircuit faults. In [21], the authors propose another distance relaying scheme for a simultaneous open conductor and ground fault. References [20] and [21] are applicable for the scenario where SC/MOVs are located at both ends of the parallel transmission lines.

In this paper, a novel fault-location method based on the distributed parameter line model for double-circuit lines is developed. The adopted model is able to accurately consider the mutual coupling between the parallel lines under the zero-sequence network, and fully takes into account the charging effect of the lines and does not lose accuracy for long lines. It utilizes unsynchronized two-terminal voltage and current phasors as inputs. The voltages and currents at the fault point are formulated in

Manuscript received February 09, 2014; revised June 08, 2014; accepted July 03, 2014. Date of publication July 29, 2014; date of current version January 21, 2015. This work was supported by the National Science Foundation under Grant ECCS-0801367. Paper no. TPWRD-00161-2014.

N. Kang is with the ABB Corporate Research Center, Raleigh, NC 27606 USA (e-mail: ning.kang@us.abb.com).

J. Chen and Y. Liao are with the Department of Electrical and Computer Engineering, University of Kentucky, Lexington, KY 40506 USA (e-mail: yliao@engr.uky.edu; jch222@uky.edu).

Digital Object Identifier 10.1109/TPWRD.2014.2337306

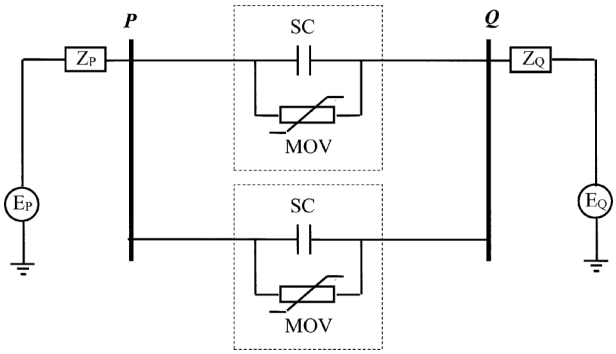

Fig. 1. Schematic diagram of a series-compensated double-circuit transmission line.

terms of the unknown fault location. Then, boundary conditions of different fault types are exploited to derive the fault-location formula. The synchronization angle is calculated using either prefault quantities or fault quantities. It is assumed that the fault impedance is purely resistive and the system is transposed. The fault type is supposedly known in advance from the terminal intelligent electronic devices (IEDs). Since the proposed method does not demand the equivalent impedance model of SC&MOV to calculate the voltage across the SC&MOV, it thus does not suffer the inaccuracy introduced in estimating the equivalent impedance of SC&MOV. The proposed method does not require the availability of the two-terminal substation impedances and is free of the impact of the fault impedance. Compared to artificial-intelligence-based methods, the proposed method does not require the training of the algorithm and can be deployed directly.

The remainder of this paper is organized as follows. Section II derives the new fault-location algorithm. Section III presents evaluation studies to validate the new method. Section IV concludes this paper.

II. Proposed Fault-Location Method

A schematic diagram of a series-compensated double-circuit transmission line is shown in Fig. 1. The prefault and during-fault voltage and current phasors from the two terminals can be retrieved from the IEDs installed at the respective substation. These measurements are communicated back to the control room computer where the fault-location application is deployed. The control room computer has access to the line parameters and upon receiving the fault measurements, executes the fault-location application and outputs the fault-location estimate for crew dispatch.

In Fig. 1, the series capacitor is installed at a fixed location on the transmission line. The MOV, equipped in parallel with SC, will conduct when an overvoltage across the series capacitor is detected. The series compensation device divides the transmission line into two sections. Since on which side the fault occurs is unknown, this paper develops two subroutines addressing a possible fault on either side. Subroutine 1 assuming the fault on the left side of the series compensation device is derived in detail and subroutine 2 assuming the fault on the opposite side is briefly described. Later on, the principle to determine the true fault-location estimation is illustrated.

A. Subroutine 1: Fault on Left Side of the Series Compensator

The notations adopted in this paper are summarized first.

P, Q	Two terminals of the series-compensated transmission line.
T	Point where the series compensation device is installed.
F	Fault point.
S	Point corresponding to the fault point on the healthy circuit.
i	Symmetrical component index; $i = 0, 1, 2$ for zero, positive, and negative sequence, respectively.
m	Unknown fault location in per unit from P to F.
l_1	Distance between P and T in kilometers.
l_2	Distance between Q and T in kilometers.
l	Total length of the transmission line in kilometers.
δ	Synchronization angle between P and Q with P as the reference.
x	Parallel line indicator; $x = 1, 2$ for each of the parallel lines.
$I_{px}^{(i)}$	ith sequence during-fault current phasor at P of line x;
$I_{qx}^{(i)}$	ith sequence during-fault current phasor at Q of line x.
$I_{sc}^{(i)}$	ith sequence during-fault current flowing through the SC&MOV bank.
$V_f^{(i)}$	ith sequence during-fault voltage at the fault point.
$V_s^{(i)}$	ith sequence during-fault voltage at the point on the healthy circuit corresponding to the fault point.
$I_f^{(i)}$	ith sequence fault current.
$I_{pf}^{(i)}$	Contribution of the fault current from P under the ith sequence network.
$I_{ps}^{(i)}$	During-fault current flowing from P to S under the ith sequence network.
$V_p^{(i)}, V_q^{(i)}$	i^{th} sequence during-fault voltage phasors at P and Q, respectively.
$z^{(i)}, y^{(i)}$	ith sequence self series-impedance and self shunt-admittance of the line per kilometer, respectively.
$z_m^{(0)}, y_m^{(0)}$	Zero-sequence mutual series impedance and mutual shunt admittance between the parallel lines per kilometer, respectively.

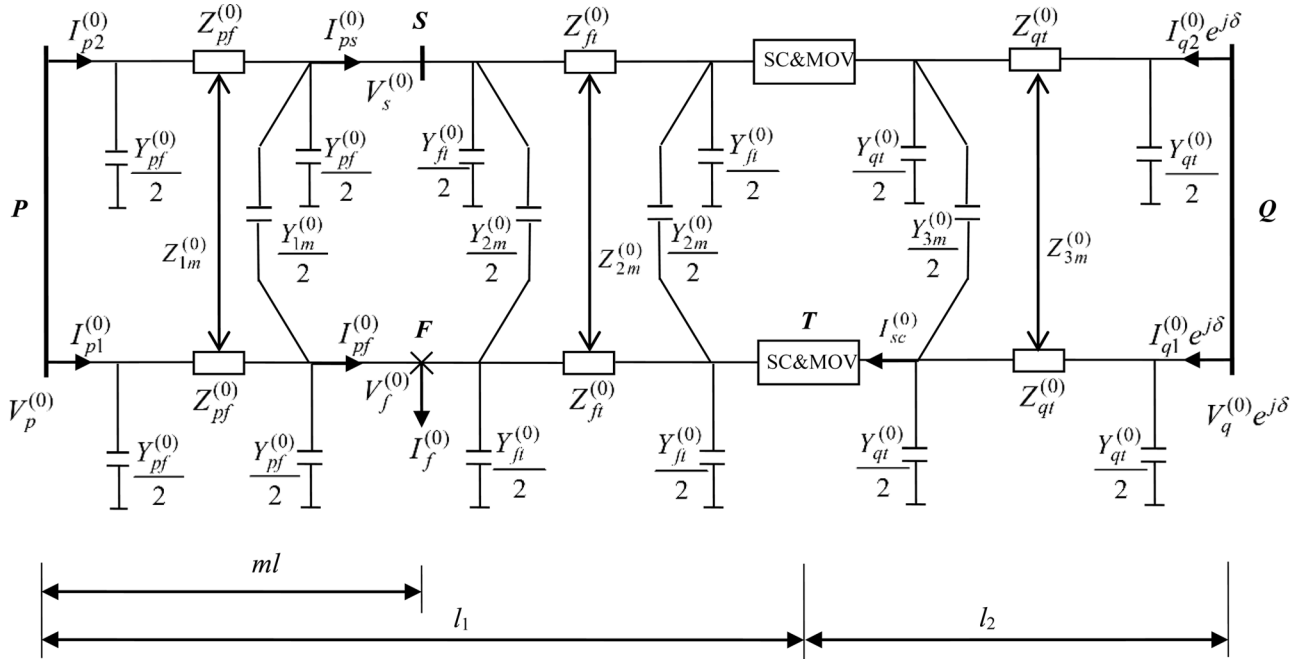

Fig. 2. Zero-sequence series-compensated double-circuit line with a fault on the left side of SC&MOV.

$Z_{pf}^{(i)}, Y_{pf}^{(i)}$ ith sequence equivalent self series-impedance and self shunt-admittance of the line between P and F, respectively.

$Z_{ft}^{(i)}, Y_{ft}^{(i)}$ ith sequence equivalent self series-impedance and self shunt-admittance of the line between F and T, respectively.

$Z_{qt}^{(i)}, Y_{qt}^{(i)}$ ith sequence equivalent self series-impedance and self shunt-admittance of the line between Q and T, respectively.

$Z_{1m}^{(0)}, Y_{1m}^{(0)}$ Zero-sequence equivalent mutual series impedance and mutual shunt admittance of the parallel lines between P and F, respectively.

$Z_{2m}^{(0)}, Y_{2m}^{(0)}$ Zero-sequence equivalent mutual series impedance and mutual shunt admittance of the parallel lines between F and T, respectively.

$Z_{3m}^{(0)}, Y_{3m}^{(0)}$ Zero-sequence equivalent mutual series impedance and mutual shunt admittance of the parallel lines between T and Q, respectively.

The schematic diagram of a zero-sequence series-compensated double-circuit line with a fault occurring to the left of the SC&MOV bank is shown in Fig. 2. The parameters including $Z_{pf}^{(0)}$, $Z_{1m}^{(0)}$, $Y_{pf}^{(0)}$, $Y_{1m}^{(0)}$, $Z_{ft}^{(0)}$, and $Z_{qt}^{(0)}$ in Fig. 2 are calculated [22] as shown in the Appendix, while the parameters, including $Z_{2m}^{(0)}$, $Y_{ft}^{(0)}$, $Y_{2m}^{(0)}$, $Z_{3m}^{(0)}$, $Y_{qt}^{(0)}$, and $Y_{3m}^{(0)}$, can be similarly derived and not shown here.

For the zero-sequence network, the following equations hold:

$$V_f^{(0)} = V_p^{(0)} - (I_{p1}^{(0)} - V_p^{(0)}\frac{Y_{pf}^{(0)}}{2})Z_{pf}^{(0)} - (I_{p2}^{(0)} - V_p^{(0)}\frac{Y_{pf}^{(0)}}{2})Z_{1m}^{(0)} \tag{1}$$

$$V_s^{(0)} = V_p^{(0)} - (I_{p2}^{(0)} - V_p^{(0)}\frac{Y_{pf}^{(0)}}{2})Z_{pf}^{(0)} - (I_{p1}^{(0)} - V_p^{(0)}\frac{Y_{pf}^{(0)}}{2})Z_{1m}^{(0)} \tag{2}$$

$$I_{pf}^{(0)} = I_{p1}^{(0)} - V_p^{(0)}\frac{Y_{pf}^{(0)}}{2} - V_f^{(0)}\frac{Y_{pf}^{(0)}}{2} - (V_f^{(0)} - V_s^{(0)})\frac{Y_{1m}^{(0)}}{2} \tag{3}$$

$$I_{ps}^{(0)} = I_{p2}^{(0)} - V_p^{(0)}\frac{Y_{pf}^{(0)}}{2} - V_s^{(0)}\frac{Y_{pf}^{(0)}}{2} - (V_s^{(0)} - V_f^{(0)})\frac{Y_{1m}^{(0)}}{2}. \tag{4}$$

Drawing on (A1)–(A6), (1)–(4) can be rearranged as

$$\begin{aligned} V_f^{(0)} = {} & V_p^{(0)}\cosh(\gamma_{m2}ml) - \frac{I_{p1}^0}{2}[Z_{cm2}\sinh(\gamma_{m2}ml) \\ & + Z_{cm1}\sinh(\gamma_{m1}ml)] \\ & - \frac{I_{p2}^{(0)}}{2}[Z_{cm2}\sinh(\gamma_{m2}ml) - Z_{cm1}\sinh(\gamma_{m1}ml)] \end{aligned} \tag{5}$$

$$\begin{aligned} V_s^{(0)} = {} & V_p^{(0)}\cosh(\gamma_{m2}ml) - \frac{I_{p1}^0}{2}[Z_{cm2}\sinh(\gamma_{m2}ml) \\ & - Z_{cm1}\sinh(\gamma_{m1}ml)] \\ & - \frac{I_{p2}^{(0)}}{2}[Z_{cm2}\sinh(\gamma_{m2}ml) + Z_{cm1}\sinh(\gamma_{m1}ml)] \end{aligned} \tag{6}$$

$$\begin{aligned} I_{pf}^{(0)} = {} & \frac{I_{p1}^{(0)}}{2}[\cosh(\gamma_{m2}ml) + \cosh(\gamma_{m1}ml)] \\ & + \frac{I_{p2}^{(0)}}{2}[\cosh(\gamma_{m2}ml) - \cosh(\gamma_{m1}ml)] \\ & - V_p^{(0)}\frac{\tanh(\frac{\gamma_{m2}ml}{2})}{Z_{cm2}}[1 + \cosh(\gamma_{m2}ml)] \end{aligned} \tag{7}$$

$$\begin{aligned} I_{ps}^{(0)} = {} & \frac{I_{p1}^{(0)}}{2}[\cosh(\gamma_{m2}ml) - \cosh(\gamma_{m1}ml)] \\ & + \frac{I_{p2}^{(0)}}{2}[\cosh(\gamma_{m2}ml) + \cosh(\gamma_{m1})] \end{aligned}$$

$$- V_p^{(0)} \frac{\tanh(\frac{\gamma_{m2} ml}{2})}{Z_{cm2}} [1 + \cosh(\gamma_{m2} ml)]. \quad (8)$$

Similarly, the current flowing through the series compensator is formulated as

$$\begin{aligned} I_{sc}^{(0)} =& \frac{1}{2} I_{q1}^{(0)} \mathbf{e}^{j\delta} [\cosh(\gamma_{m2} l_2) + \cosh(\gamma_{m1} l_2)] \\ &+ \frac{1}{2} I_{q2}^{(0)} \mathbf{e}^{j\delta} [\cosh(\gamma_{m2} l_2) - \cosh(\gamma_{m1} l_2)] \\ &- V_q^{(0)} \mathbf{e}^{j\delta} \frac{\tanh(\frac{\gamma_{m2} l_2}{2})}{Z_{cm2}} [1 + \cosh(\gamma_{m2} l_2)]. \end{aligned} \quad (9)$$

Equations (5)–(8) show that $V_f^{(0)}$, $V_s^{(0)}$, $I_{pf}^{(0)}$, and $I_{ps}^{(0)}$ are expressed in terms of $V_p^{(0)}$, $I_{p1}^{(0)}$, $I_{p2}^{(0)}$, and m. Equation (9) indicates that $I_{sc}^{(0)}$ is expressed with respect to $V_q^{(0)}$, $I_{q1}^{(0)}$, and $I_{q2}^{(0)}$.

For the positive- or negative-sequence network, the formulations of $I_f^{(i)}$, $V_f^{(i)}$, $I_{pf}^{(i)}$, and $I_{sc}^{(i)}$ $(i = 1, 2)$ are the same as the single-circuit lines and are directly shown here [13]. See (10)–(13) at the bottom of the page, where

$$Z_c^{(i)} = \sqrt{\frac{z^{(i)}}{y^{(i)}}}$$
$$\gamma^{(i)} = \sqrt{z^{(i)} y^{(i)}}.$$

Equations (10)–(12) show that $I_f^{(i)}$, $V_f^{(i)}$, and $I_{pf}^{(i)}$ are expressed in terms of $V_p^{(i)}$, $V_q^{(i)}$, $I_{p1}^{(i)}$, $I_{q1}^{(i)}$, and m. Equation (13) shows that $I_{sc}^{(i)}$ is expressed with respect to $V_q^{(i)}$ and $I_{q1}^{(i)}$.

Next, the fault-location formulas for different fault types are derived.

1) LG Fault: For an AG fault, the following boundary condition holds:

$$I_f^{(0)} = I_f^{(1)} = I_f^{(2)}. \quad (14)$$

Let $i = 1, 2$ in (10) and the expressions of $I_f^{(1)}$ and $I_f^{(2)}$ can be obtained. Substituting the aforementioned explicit expressions of $I_f^{(1)}$ and $I_f^{(2)}$ into $I_f^{(1)} = I_f^{(2)}$ and taking advantage of $\gamma^{(1)} = \gamma^{(2)}$, it is observed that the unknown fault location is eliminated and the synchronization angle can be computed as follows [19]:

$$\mathbf{e}^{j\delta} = - \frac{(I_{p1}^{(1)} - I_{p1}^{(2)}) \cosh(\gamma^{(1)} l_1) - \frac{(V_p^{(1)} - V_p^{(2)})}{Z_c^{(1)}} \sinh(\gamma^{(1)} l_1)}{(I_{q1}^{(1)} - I_{q1}^{(2)}) \cosh(\gamma^{(1)} l_2) - \frac{(V_q^{(1)} - V_q^{(2)})}{Z_c^{(1)}} \sinh(\gamma^{(1)} l_2)}. \quad (15)$$

Further, the following equation exists for an AG fault:

$$V_f^{(1)} + V_f^{(2)} + V_f^{(0)} = 3 R_f I_f^{(1)} \quad (16)$$

where $V_f^{(1)}$, $V_f^{(2)}$, and $V_f^{(0)}$ can be obtained from (5) and (11) and $I_f^{(1)}$ can be obtained from (10). Since R_f is a real number, it indicates that $(V_f^{(1)} + V_f^{(2)} + V_f^{(0)})$ and $I_f^{(1)}$ are in phase. Therefore, the following equation can be reached:

$$\mathrm{Im}\{\frac{V_f^{(1)} + V_f^{(2)} + V_f^{(0)}}{I_f^{(1)}}\} = 0 \quad (17)$$

where $\mathrm{Im}(\cdot)$ yields the imaginary part of the argument.

In (17), the synchronization angle is acquired using (15), and the only unknown variable is the fault location. The iterative approach, such as Newton-Raphson can be harnessed to pinpoint the fault location. The initial value for the fault location can be chosen as 0.5 p.u. to initialize the iteration process. The fault-location estimate is considered converged when the difference in the fault-location estimate between two iterations is smaller than the specified tolerance.

2) LL Fault: For a BC fault, the following two equations exist:

$$I_f^{(1)} = - I_f^{(2)} \quad (18)$$
$$V_f^{(1)} - V_f^{(2)} = R_f I_f^{(1)}. \quad (19)$$

Similar to AG faults, from (18), the synchronization angle can be calculated as follows:

$$\boldsymbol{e}^{j\delta} = - \frac{(I_{p1}^{(1)} + I_{p1}^{(2)}) \cosh(\gamma^{(1)} l_1) - \frac{(V_p^{(1)} + V_p^{(2)})}{Z_c^{(1)}} \sinh(\gamma^{(1)} l_1)}{(I_{q1}^{(1)} + I_{q1}^{(2)}) \cosh(\gamma^{(1)} l_2) - \frac{(V_q^{(1)} + V_q^{(2)})}{Z_c^{(1)}} \sinh(\gamma^{(1)} l_2)}. \quad (20)$$

$$I_f^{(i)} = \frac{I_{p1}^{(i)} \cosh(\gamma^{(i)} l_1) + I_{q1}^{(i)} \mathbf{e}^{j\delta} \cosh(\gamma^{(i)} l_2) - \frac{V_p^{(i)}}{Z_c^{(i)}} \sinh(\gamma^{(i)} l_1) - \frac{V_q^{(i)} \mathbf{e}^{j\delta}}{Z_c^{(i)}} \sinh(\gamma^{(i)} l_2)}{\cosh[\gamma^{(i)} (l_1 - ml)]} \quad (10)$$

$$V_f^i = V_p^{(i)} \cosh(\gamma^{(i)} ml) - I_{p1}^{(i)} Z_c^{(i)} \sinh(\gamma^{(i)} ml) \quad (11)$$

$$I_{pf}^{(i)} = I_{pi}^{(i)} \cosh(\gamma^{(i)} ml) - \frac{V_p^{(i)}}{Z_c^{(i)}} \sinh(\gamma^{(i)} ml) \quad (12)$$

$$I_{sc}^{(i)} = I_{q1}^{(i)} \mathbf{e}^{j\delta} \cosh(\gamma^{(i)} l_2) - \frac{V_q^{(i)} \mathbf{e}^{j\delta}}{Z_c^{(i)}} \sinh(\gamma^{(i)} l_2) \quad (13)$$

Based on (19), the fault location can be determined from the following formula:

$$\mathrm{Im}\{\frac{V_f^{(1)}-V_f^{(2)}}{I_f^{(1)}}\}=0. \tag{21}$$

3) LLL Fault: For a three-phase fault, the synchronization angle can only be acquired from the prefault measurements as follows [19]:

$$e^{j\delta}=-\frac{I_{p1}^{(1)0}\cosh(\gamma^{(1)}l_1)-\frac{V_p^{(1)0}}{Z_c^{(1)}}\sinh(\gamma^{(1)}l_1)}{I_{q1}^{(1)0}\cosh(\gamma^{(1)}l_2)-\frac{V_q^{(1)0}}{Z_c^{(1)}}\sinh(\gamma^{(1)}l_2)}. \tag{22}$$

Here, $V_p^{(1)0}$ and $I_{p1}^{(1)0}$ represent the prefault positive-sequence voltage and current phasors at P. $V_q^{(1)0}$ and $I_{q1}^{(1)0}$ denote the prefault positive-sequence voltage and current phasors at Q. Note the acquisition of the synchronization angle using (22) is also applicable to other kinds of faults. The condition at the fault point is expressed by the following equation:

$$V_f^{(1)}=R_f I_f^{(1)}. \tag{23}$$

Utilizing (10), (11), and (23), the fault-location formula is attained as

$$\mathrm{Im}\{\frac{V_f^{(1)}}{I_f^{(1)}}\}=0. \tag{24}$$

4) LLG Fault: For a BCG fault, the following relationship is satisfied at the fault point:

$$V_f^{(0)}-V_f^{(1)}=3R_f I_f^{(0)}. \tag{25}$$

The synchronization angle can be calculated using the prefault measurements as in (22). Based on (25), the fault location can be derived from the following equation:

$$\mathrm{Im}\{\frac{V_f^{(0)}-V_f^{(1)}}{I_f^{(0)}}\}=0 \tag{26}$$

where

$$I_f^{(0)}=-(I_f^{(1)}+I_f^{(2)})$$

and $I_f^{(1)}$ and $I_f^{(2)}$ can be obtained from (10).

Fault-location formulas for fault types involving other phases can be similarly deduced by utilizing the respective boundary conditions and are not shown here.

It should be pointed out that when synchronized measurements of the two terminals are available from phasor measurement units (PMUs), the fault-location formulations derived here are still applicable with the synchronization angle being set to zero.

The fault-location formulas for Subroutine 2 where the fault occurs on the right side of the series compensator can be similarly derived and are not shown here.

B. Fault-Location Identification Method

Various methods to select the valid subroutine have been proposed and they all work properly [9], [11]. Based on these approaches, the fault-location identification method suitable to this paper is proposed. Suppose that the two solutions from the two subroutines are denoted as m_1 and m_2. The fault-location estimate can be judged as true only when it satisfies the following three principles:

1) The fault-location estimate is within the assumed range.
2) The fault resistance takes a non-negative value.
3) The equivalent impedances of the series compensation device for all three phases have a non-negative real part and negative imaginary part, that is, $\mathrm{Re}\{Z_{eq\_x}\}\geq 0$ and $\mathrm{Im}\{Z_{eq\_x}\}<0$, $x=a,b,c$.

As for principle 1, the assumed range for m_1 is $[0, l_1/l]$ and that for m_2 is $[l_1/l, 1]$. With the fault location being known, (16), (19), (23), and (25) can be used to calculate the fault resistances for AG, BC, ABC, and BCG faults, respectively. The A-phase equivalent impedance of the series device for subroutine 1 can be formulated as

$$Z_{eq\_a}=\frac{(V_{sc\_r}^{(0)}-V_{sc\_l}^{(0)})+(V_{sc\_r}^{(1)}-V_{sc\_l}^{(1)})+(V_{sc\_r}^{(2)}-V_{sc\_l}^{(2)})}{I_{sc}^{(0)}+I_{sc}^{(1)}+I_{sc}^{(2)}} \tag{27}$$

where $V_{sc\_l}^{(i)}$ and $V_{sc\_r}^{(i)}$ $(i=0,1,2)$ denote the voltage at the left and right side of the series compensator, respectively. Utilizing the calculated fault-location estimate and the two-terminal voltage and current measurements, the quantities in (27) can be calculated. $I_{sc}^{(0)}$ can be calculated from (9) and $I_{sc}^{(i)}$ $(i=1,2)$ can be obtained from (13). $V_{sc\_r}^{(i)}$ and $V_{sc\_l}^{(i)}$ $(i=1,2)$ can be attained as follows:

$$V_{sc\_r}^{(i)}=V_q^{(i)}e^{j\delta}\cosh(\gamma^{(i)}l_2)-I_{q1}^{(i)}e^{j\delta}Z_c^{(i)}\sinh(\gamma^{(i)}l_2) \tag{28}$$

$$V_{sc\_l}^{(i)}=V_f^{(i)}\cosh(\gamma^{(i)}(l_1-ml))-(I_{pf}^{(i)}-I_f^{(i)})Z_c^{(i)}\sinh(\gamma^{(i)}(l_1-ml)) \tag{29}$$

where $I_f^{(i)}$, $V_f^{(i)}$, and $I_{pf}^{(i)}$ can be acquired from (10)–(12). Moreover, $V_{sc\_r}^{(0)}$ and $V_{sc\_l}^{(0)}$ in (27) can be written as

$$\begin{aligned}V_{sc\_r}^{(0)}=&V_q^{(0)}e^{j\delta}\cosh(\gamma_{m2}l_2)\\&-\frac{1}{2}I_{q1}^{(0)}e^{j\delta}[Z_{cm2}\sinh(\gamma_{m2}l_2)+Z_{cm1}\sinh(\gamma_{m1}l_2)]\\&-\frac{1}{2}I_{q2}^{(0)}e^{j\delta}[Z_{cm2}\sinh(\gamma_{m2}l_2)-Z_{cm1}\sinh(\gamma_{m1}l_2)]\end{aligned} \tag{30}$$

$$\begin{aligned}V_{sc\_l}^{(0)}=&V_f^{(0)}-[I_{pf}^{(0)}-I_f^{(0)}-V_f^{(0)}\frac{Y_{fr}^{(0)}}{2}-(V_f^{(0)}-V_s^{(0)})\frac{Y_{2m}^{(0)}}{2}]Z_{fr}^{(0)}\\&-[I_{ps}^{(0)}-V_s^{(0)}\frac{Y_{fr}^{(0)}}{2}-(V_s^{(0)}-V_f^{(0)})\frac{Y_{2m}^{(0)}}{2}]Z_{2m}^{(0)}\end{aligned} \tag{31}$$

where $V_f^{(0)}$, $V_s^{(0)}$, $I_{pf}^{(0)}$, and $I_{ps}^{(0)}$ can be gained from (5)–(8). $I_f^{(0)}$ in (31) can be calculated using boundary conditions for different types of fault, that is, $I_f^{(0)}=-(I_f^{(1)}+I_f^{(2)})$ for BCG faults and $I_f^{(0)}=I_f^{(1)}$ for AG faults. For BC and ABC faults, $I_f^{(0)}=0$.

The equivalent impedances of the series compensation device for phase B and C can be deduced similarly.

The computation of the three-phase equivalent impedances of the series device for subroutine 2 is very similar and not shown here. The subroutine that satisfies all of the three principles should be selected and its fault-location estimate should be regarded as the true fault-location estimate.

III. Evaluation Studies

This section presents the simulation results to evaluate the developed fault-location method. The proposed fault-location algorithms and the fault-location identification method are implemented as a Matlab script. Matlab SimPowerSystems[23] is utilized to simulate the series-compensated double-circuit line and generate two-terminal voltage and current phasors for faults of different types, locations, and resistances. The Matlab script reads the simulated measurements from Matlab SimPowerSystems and outputs the unique fault-location estimate for each specific fault. The accuracy of the fault-location estimate is evaluated by percentage error defined as

$$\%\text{Error} = \frac{|\text{Actual Location -Estimated Location}|}{\text{Total Length of Faulted Line}} \times 100. \quad (32)$$

The sample power system studied has a configuration as shown in Fig. 1 and is a 500-kV, 1000-MVA, 50-Hz double-circuit transmission line compensated at the degree of 45%. The total length of the line is 350 km, with the series compensation device installed at 200 km (0.5714 p.u.) from terminal P. The synchronization angle is set to 22.5°. Voltage source data and transmission-line parameters are shown in Tables V and VI. MOV modeling is referred to in the Appendix.

Typical fault-location results yielded by the proposed method are presented in Table I. The first two columns display the actual fault type and fault resistance simulated. The remaining columns present the percentage fault-location error under various actual fault locations. The scope of the proposed fault-location method is limited to faults within one circuit and is not applicable to intercircuit faults. The fault types throughout this paper refer to faults within a single circuit.

From Table I, it can be observed that the fault-location result is highly accurate, with the largest error being 0.0485%. In general, the bigger the fault resistance, the larger the fault-location error.

TABLE I
Fault-Location Results

Fault Type	Fault Res. (ohm)	Fault-Location Error (%)				
		15km	120km	180km	260km	320km
AG	0	0.0009	0.0116	0.0357	0.0052	0.0002
	1	0.0010	0.0115	0.0356	0.0055	0.0001
	10	0.0012	0.0118	0.0364	0.0052	0.0002
	50	0.0025	0.0160	0.0400	0.0054	0.0001
	100	0.0037	0.0183	0.0485	0.0058	0.0003
BC	0	0.0006	0.0010	0.0030	0.0008	0.0003
	1	0.0006	0.0010	0.0032	0.0009	0.0002
	10	0.0010	0.0016	0.0038	0.0004	0.0005
	50	0.0025	0.0042	0.0068	0.0012	0.0008
	100	0.0044	0.0090	0.0122	0.0031	0.0014
BCG	0	0.0006	0.0094	0.0295	0.0045	0.0003
	1	0.0005	0.0093	0.0296	0.0046	0.0002
	10	0.0003	0.0094	0.0297	0.0042	0.0006
	50	0.0001	0.0109	0.0326	0.0025	0.0027
	100	0.0007	0.0127	0.0372	0.0025	0.0026
ABC	0	0.0003	0.0007	0.0032	0.0001	0.0005
	1	0.0004	0.0008	0.0033	0.0001	0.0005
	10	0.0013	0.0014	0.0039	0.0001	0.0005
	50	0.0037	0.0051	0.0080	0.0007	0.0005
	100	0.0064	0.0116	0.0212	0.0029	0.0009

TABLE II
Fault-Location Results With Error in Pos. Seq. Imp

Fault Type	Fault-Location Error (%)
AG	1.71
BC	4.60
BCG	2.25
ABC	4.59

TABLE III
Fault-Location Results for Untransposed Lines

Fault Type	Fault-Location Error (%)
AG	0.24
BC	1.00
BCG	0.62
ABC	0.09

A. Impact of Line Parameter Errors

To observe the impact of possible line parameter errors over the fault-location accuracy, Table II shows the fault-location results with 10% error in the positive-sequence line impedance. The actual fault location is fixed at 180 km and the actual fault resistance is 10 Ω. It can be observed that the biggest error in Table II is 4.60% and is still acceptable. Research on how to obtain accurate line parameters for an enhanced fault-location estimate may be performed in the future.

B. Impact of the Untransposition of Lines

To study the impacts of untransposition of lines on fault-location estimate, Table III shows the fault-location results when applying the proposed method to untransposed lines. The actual fault-location is fixed at 120 km and the actual fault resistance is 50 Ω. It can be observed that untransposition causes certain errors in fault location, but the results are still quite accurate.

C. Impact of Measurement Errors

The proposed fault-location algorithm utilizes fundamental frequency phasors, so factors, such as possible measurement errors due to current transformers (CTs) and potential transformers (PTs), such as capacitor voltage transformers, that affect phasor accuracy may adversely impact fault-location accuracy. This section reports sample results on the impacts of potential voltage and current measurement errors on the fault-location estimate.

The proposed method is desirably insensitive to possible voltage and current measurement errors. As examples, in

TABLE IV
FAULT-LOCATION RESULTS WITH MEASUREMENT ERRORS

Measurement Type	Fault-Location Error (%)			
	AG	BC	BCG	ABC
Current	0.3906	0.3888	0.3908	0.3890
Voltage	0.4295	0.4294	0.4293	0.4291

Table IV, the fault-location results with 10% error in the local faulted line current measurements and 10% error in the local voltage measurements are reported, respectively. The actual fault location is 15 km, and the actual fault resistance is 0 Ω. As evinced, the fault-location results are still quite satisfactory.

D. Illustration of the Fault-Location Identification Method

As stated in Section II-B, it is necessary to determine on which side of the compensator the fault occurs. In the following section, two cases will be used as examples to illustrate this process.

1) Case 1: AG Fault; Actual Fault Location is 60 km (0.1714 p.u.) and Actual Fault Resistance is 1 Ω (0.0040 p.u.): The two fault-location estimates gained from the two subroutines are $m_1 = 0.1715$ p.u. and $m_2 = 0.4730$ p.u.

Since m_2 falls outside $[0.5714, 1]$ p.u., it is filtered out. The fault resistance and three-phase equivalent impedances corresponding to m_1 are further examined as follows:

$$R_{f1} = 0.004 \text{ p.u.},\ Z_{eq\_a1} = 0.0204 - j0.2159,$$
$$Z_{eq\_b1} = 0 - j0.2192,\ Z_{eq\_c2} = 0 - j0.2113.$$

Since all three principles as outlined in Section II-B are satisfied for the solution of subroutine 1, the true fault location is determined to be 0.1715 p.u.

2) Case 2: ABC Fault; Actual Fault Location is 180 km (0.5143 p.u.) and Actual Fault Resistance is 10 Ω (0.040 p.u.): The two fault-location estimates yielded from the two subroutines are $m_1 = 0.5143$ p.u. and $m_2 = 0.7662$ p.u.

Since they both satisfy principle 1, the two corresponding fault resistances are further calculated as $R_{f1} = 0.04$ p.u. and $R_{f2} = 0.956$ p.u.

The fact that both fault resistances are positive numbers implies that it is necessary to calculate the three-phase equivalent impedances corresponding to both fault-location estimates. The values are

$$\begin{aligned} Z_{eq\_a1} &= 0.0737 - j0.1323, \\ Z_{eq\_b1} &= 0.0737 - j0.1323, \\ Z_{eq\_c1} &= 0.0737 - j0.1323. \\ Z_{eq\_a2} &= -0.1562 - j0.1399, \\ Z_{eq\_b2} &= -0.1562 - j0.1399, \\ Z_{eq\_c2} &= -0.1562 - j0.1399. \end{aligned}$$

It can be seen that only the solution from subroutine 1 satisfies all of the three principles and, therefore, it is concluded that the true fault location is 0.5143 p.u..

The method to identify which side of the compensator that the fault truly occurs on has been shown to be valid and effective.

TABLE V
VOLTAGE SOURCE DATA

Quantity	Source P	Source Q
Emf(p.u.)	$1.0\angle 20^\circ$	$1.0\angle 0^\circ$
Pos. Seq. Imp. (Ω)	17.177+j45.5285	15.31+j45.9245
Zero. Seq. Imp. (Ω)	2.5904+j14.7328	0.7229+j15.1288

TABLE VI
TRANSMISSION-LINE DATA

Parameters	Pos. Seq	Zero. Seq	Zero. Seq Mutual
R(Ω/km)	0.061	0.268	0.12
L(mH/km)	1.1182	3.3012	1.1485
C(nF/km)	14.8332	8.6001	-0.6761

IV. CONCLUSION

This paper presents a new method to pinpoint fault location on series-compensated double-circuit lines. Unsynchronized voltage and current phasors from both terminals of the line are utilized. The distributed parameter line model is harnessed that fully considers the effect of shunt capacitances of the line.

Two subroutines are developed to determine the possible locations of the fault on both sides of the series compensation device. A fault-location identification method is then applied to identify the true fault distance. The synchronization angle can be acquired independently using either prefault measurements for all types of faults or fault measurements for LG and LL faults, and be employed in the fault-location derivation. Evaluation studies based on simulations have demonstrated that the proposed fault-location algorithm is highly accurate and the fault-location identification method is valid.

APPENDIX

Parameters in Fig. 2:

$$Z_{pf}^{(0)} = \frac{1}{2}[Z_{cm2}\sinh(\gamma_{m2}ml) + Z_{cm1}\sinh(\gamma_{m1}ml)] \quad \text{(A1)}$$

$$Z_{1m}^{(0)} = \frac{1}{2}[Z_{cm2}\sinh(\gamma_{m2}ml) - Z_{cm1}\sinh(\gamma_{m1}ml)] \quad \text{(A2)}$$

$$Y_{pf}^{(0)} = \frac{2\tanh(\frac{\gamma_{m2}ml}{2})}{Z_{cm2}} \quad \text{(A3)}$$

$$Y_{1m}^{(0)} = \frac{\tanh(\frac{\gamma_{m1}ml}{2})}{Z_{cm1}} - \frac{\tanh(\frac{\gamma_{m2}ml}{2})}{Z_{cm2}} \quad \text{(A4)}$$

$$Z_{ft}^{(0)} = \frac{1}{2}\{Z_{cm2}\sinh[\gamma_{m2}(l_1 - ml)] + Z_{cm1}\sinh[\gamma_{m1}(l_1 - ml)]\} \quad \text{(A5)}$$

$$Z_{qt}^{(0)} = \frac{1}{2}[Z_{cm2}\sinh(\gamma_{m2}l_2) + Z_{cm1}\sinh(\gamma_{m1}l_2)] \quad \text{(A6)}$$

where

$$Z_{cm1} = \sqrt{\frac{(z^{(0)} - z_m^{(0)})}{(y^{(0)} + 2y_m^{(0)})}}$$

$$Z_{cm2} = \sqrt{\frac{(z^{(0)} + z_m^{(0)})}{y^{(0)}}}$$
$$\gamma_{m1} = \sqrt{(z^{(0)} - z_m^{(0)})(y^{(0)} + 2y_m^{(0)})}$$
$$\gamma_{m2} = \sqrt{(z^{(0)} + z_m^{(0)})y^{(0)}}.$$

MOV Modeling:

The MOV consists of 30 columns of metal–oxide discs connected in parallel inside the same porcelain housing. The characteristic of each column is represented by a combination of three exponential functions [23]

$$\frac{V}{V_{\text{ref}}} = k_i(\frac{I}{I_{\text{ref}}})^{1/\alpha_i} \tag{A7}$$

where

$$V_{\text{ref}} = 165\ \text{kV},\ I_{\text{ref}} = 1\ \text{kA},\ i = 1, 2, 3.$$

The parameters of the three segments of (A7) are $k_1 = 0.955$, $\alpha_1 = 50$, $k_2 = 1.0$, $\alpha_2 = 25$, $k_3 = 0.9915$, and $\alpha_3 = 16.5$

REFERENCES

[1] M. Avendaño-Mora and J. V. Milanovic, "Generalized formulation of the optimal monitor placement problem for fault location," *Elect. Power Syst. Res.*, vol. 93, no. 12, pp. 120–126, Dec. 2012.

[2] C. A. Apostolopoulos and G. N. Korres, "A novel algorithm for locating faults on transposed/untransposed transmission lines without utilizing line parameters," *IEEE Trans. Power Del.*, vol. 25, no. 4, pp. 2328–2338, Oct. 2010.

[3] G. Preston, Z. M. Radojevic, C. H. Kim, and V. Terzija, "New settings-free fault location algorithm based on synchronised sampling," *IET Gen. Transm. Distrib.*, vol. 5, no. 3, pp. 376–383, Mar. 2011.

[4] M. G. Ahsaee and J. Sadeh, "A novel fault-location algorithm for long transmission lines compensated by series FACTS devices," *IEEE Trans. Power Del.*, vol. 26, no. 4, pp. 2299–2308, Oct. 2011.

[5] S. G. Srivani and T. T. Nisha, "Estimation of fault location algorithm in series compensated FACT systems," in *Proc. IEEE 5th Power India Conf.*, 2012, pp. 1–5.

[6] Y. Wang, X. Yin, Z. Zhang, J. Tang, and Z. He, "A new method for identifying the fault location on series compensated lines based on transient fault information," in *Proc. 4th Int. Conf. Elect. Utility Dereg. Restruct. Power Technol.*, 2011, pp. 78–82.

[7] M. M. Saha, J. Izykowski, E. Rosolowski, and B. Kasztenny, "A new accurate fault locating algorithm for series compensated lines," *IEEE Trans. Power Del.*, vol. 14, no. 3, pp. 789–797, Jul. 1999.

[8] J. Sadeh, N. Hadjsaid, A. M. Ranjbar, and R. Feuillet, "Accurate fault location algorithm for series compensated transmission lines," *IEEE Trans. Power Del.*, vol. 15, no. 3, pp. 1027–1033, Jul. 2000.

[9] M. Kizilcay and P. L. Seta, "A new unsynchronized two-terminals fault location method on series compensated lines," in *Proc. IEEE Russia Power Tech Conf.*, Russia, 2005, pp. 1–7.

[10] M. Al-Dabbagh and S. K. Kapuduwage, "Using instantaneous values for estimating fault locations on series compensated transmission lines," *Elect. Power Syst. Res.*, vol. 76, pp. 25–32, 2005.

[11] C.-S. Yu, C.-W. Liu, S.-L. Yu, and J.-A. Jiang, "A new PMU-based fault location algorithm for series compensated lines," *IEEE Trans. Power Del.*, vol. 17, no. 1, pp. 33–46, Jan. 2002.

[12] R. Razzaghi, G. Lugrin, M. Paolone, and F. Rachidi, "On the use of electromagnetic time reversal to locate faults in series-compensated transmission lines," in *Proc. IEEE Power Tech*, 2013, pp. 1–5.

[13] N. Kang and Y. Liao, "New fault location technique for series compensated transmission lines," *Int. Rev. Elect. Eng.*, vol. 4, no. 6, pp. 1385–1390, Dec. 2009.

[14] D. Novosel, B. Bachmann, Y. Hu, and M. M. Saha, "Algorithms for locating faults on series compensated lines using neural network and deterministic methods," *IEEE Trans. Power Del.*, vol. 11, no. 4, pp. 1728–1736, Oct. 1996.

[15] W. J. Cheong and R. K. Aggarwal, "A novel fault location technique based on current signals only for thryister controlled series compensated transmission lines using wavelet analysis and self organising map neural networks," in *Proc. 8th IEE Int. Conf. Develop. Power Syst. Protect.*, 2004, vol. 1, pp. 224–227.

[16] P. Ray, B. K. Panigrahi, and N. Senroy, "Hybrid methodology for fault distance estimation in series compensated transmission line," *IET Gen. Transm. Distrib.*, vol. 7, no. 5, pp. 431–439, 2013.

[17] T. Maekawa, Y. Obata, M. Yamaura, Y. Kurosawa, and H. Takani, "Fault location for series compensated parallel lines," in *Proc. Transm. Distrib. Conf. Exhibit.: Asia Pacific*, Oct. 2002, pp. 824–829.

[18] M. M. Saha, K. Wikstrom, J. Izykowski, and E. Rosolowski, "New concept for fault location in series-compensated parallel lines," in *Proc. IEEE Power Eng. Soc. Winter Meeting*, Feb. 2001, vol. 2, pp. 769–774.

[19] J. Izykowski, E. Rosolowski, P. Balcerek, M. Fulczyk, and M. M. Saha, "Fault location on double-circuit series-compensated lines using two-end unsynchronized measurements," *IEEE Trans. Power Del.*, vol. 26, no. 4, pp. 2072–2080, Oct. 2011.

[20] V. H. Makwana and B. R. Bhalja, "A new adaptive distance relaying scheme for mutually coupled series-compensated parallel transmission lines during intercircuit faults," *IEEE Trans. Power Del.*, vol. 26, no. 4, pp. 2726–2734, Oct. 2011.

[21] V. H. Makwana and B. R. Bhalja, "A new digital distance relaying scheme for series-compensated double-circuit line during open conductor and ground fault," *IEEE Trans. Power Del.*, vol. 27, no. 2, pp. 910–917, Apr. 2012.

[22] N. Kang and Y. Liao, "Equivalent PI circuit for zero-sequence double circuit transmission lines," in *Proc. IEEE Power Eng. Soc. Gen. Meeting*, San Diego, CA, USA, Jul. 2012, pp. 1–7.

[23] *"Matlab SimPowerSystems Help Documentation,"* MathWorks Inc., Natick, MA, USA, 2013.

Ning Kang (M'10) received the Ph.D. degree in electrical engineering from the University of Kentucky, Lexington, KY, USA, in 2010.

Currently, she is a Senior R&D Engineer with the ABB Corporate Research Center, Raleigh, NC, USA. Her research interests include protection, power-quality analysis, large-scale resource scheduling optimization, fault diagnosis, asset management, and power system modeling and simulation.

Jiaxiong Chen (M'13) received the Ph.D. degree in electrical and computer engineering from the University of Kentucky, Lexington, KY, USA in 2013.

His research field is power system state estimation and fault-location detection.

Yuan Liao (S'98–M'00–SM'05) is currently an Associate Professor with the Department of Electrical and Computer Engineering at the University of Kentucky, Lexington, KY, USA. He is also the Director of the Graduate Certificate of the Power and Energy Institute of Kentucky (PEIK), University of Kentucky, Lexington, KY, USA.

His research interests include protection, power-quality analysis, large-scale resource scheduling optimization, and Network Management System/Supervisory Control and Data Acquisition System design.